


Planar-Biaxial Thermo-mechanical Fatigue Behavior of Nickel-Base Superalloy Inconel 718 Under Proportional Loading



MARCO BÖCKER, HARISH RAMESH BABU, SEBASTIAN HENKEL,
MARIO RADDATZ, UWE GAMPE, and HORST BIERMANN 

The planar-biaxial thermo-mechanical fatigue behavior of nickel-base superalloy Inconel 718 was studied for selected proportional loading conditions, in particular biaxial strain ratios of 1.0, 0.6, and -1.0 . The cyclic temperature loading with minimum and maximum temperatures of $400\text{ }^{\circ}\text{C}$ and $630\text{ }^{\circ}\text{C}$ and a duration of 250 seconds was either In-Phase or Out-of-Phase to the mechanical axes. Besides the multiaxial tests, uniaxial thermo-mechanical fatigue tests were conducted In-Phase and Out-of-Phase with the same temperature cycle and cycle duration. The performed thermo-mechanical fatigue tests were analyzed regarding the deformation and lifetime behavior and compared with high-temperature isothermal low-cycle fatigue tests from a previous work of the authors. On the side of the lifetime description, a strain- and a stress-based approach were presented. For the planar-biaxial tests, the crack initiation mechanism and crack paths were shown.

<https://doi.org/10.1007/s11661-022-06885-x>
© The Author(s) 2022

I. INTRODUCTION

SUPERALLOY Inconel 718® (IN718) is a common choice for many structural applications, which have to be exposed to high temperatures up to approximately $650\text{ }^{\circ}\text{C}$ and simultaneously applied mechanical loads. These loads can cause damage to the material that finally may lead to the failure of the component. Hence, the knowledge of the resistance of the material is of high interest. While many fatigue-related design decisions rely on data of uniaxial quasi-static, isothermal (LCF), and thermo-mechanical fatigue (TMF) tests, the influence of more complex and multiaxial fatigue loads, as they occur in service of *e.g.*, turbine disks, is not that frequently investigated and described in detail. This results in an absence of important design specifications, calculation uncertainties, and thus additional added safety factors.

Multiaxial loads often have a high influence on the structural integrity of components. Calculations of Waldren *et al.*^[1] for fast rotating turbine disks showed that high principal biaxial loads in the tangential and radial directions occur. In their experimental investigations, quasi-static failure of a rotating steel disk occurred under biaxial tension.

Due to non-constant loading conditions of such multiaxially loaded components, for example, start-up and shutdown procedures or different power demands, the applied materials are consequently exposed to complex multiaxial thermo-mechanical fatigue cycles.

For IN718, it was found that multiaxial fatigue loading has a major influence on the TMF damage and lifetime behavior.^[2] Since fatigue crack initiation in IN718 under TMF load is most likely to occur right at or close to the surface,^[3] the influence of service-relevant multiaxial loading states at the surface on the thermo-mechanical fatigue lifetime has to be studied. On surfaces, a plane stress state is assumed and the multiaxial loading state can be expressed by two principal strain parameters on the surface plane ε_1 and ε_2 and their orientations.

The type of biaxial loading is frequently expressed by the biaxial ratio Φ (Eq. [1]) with a minimum value of -1 , which is pure shear, and a maximum value of 1 , which describes equi-biaxial load.

$$\Phi = \frac{\varepsilon_2}{\varepsilon_1} \text{ with } |\varepsilon_1| \geq |\varepsilon_2| \quad [1]$$

MARCO BÖCKER, SEBASTIAN HENKEL, and HORST BIERMANN are with the Technische Universität Bergakademie Freiberg, Institute of Materials Engineering, Gustav-Zeuner-Straße 5, 09599 Freiberg, Germany. Contact e-mail: marco.boecker@iwt.tu-freiberg.de HARISH RAMESH BABU, MARIO RADDATZ, and UWE GAMPE are with the Technische Universität Dresden, Institute of Power Engineering, Helmholtzstraße 14, 01069 Dresden, Germany. Manuscript submitted August 26, 2022; accepted October 25, 2022.

Article published online November 25, 2022

If the biaxial ratio Φ is constant and the principal stress/strain system is not rotating over time within the cycle, the fatigue load is considered proportional. Under uniaxial load ε_1 , the principal strain in the orthogonal direction ε_2 is introduced by the materials' transverse contraction, calculated by the use of the Poisson ratio ν (Eq. [2]), which results in a biaxial ratio of $\Phi = -\nu$.

$$\varepsilon_2 = -\varepsilon_1 \nu \quad [2]$$

In rotating turbine disks, higher biaxial ratios Φ occur. While most multiaxial investigations are performed using tension–torsion setups, higher biaxial ratios than that of the uniaxial case cannot be executed. Although low biaxial ratios are relevant for many applications, the influence of higher biaxial ratios than $\Phi > -\nu$ on material behavior cannot be investigated using those systems.^[4] Here, a reasonable approach is the usage of planar-biaxial setups, which are significantly more complex than tension–torsion tests, but less complex and cheaper than component-like spin tests. In planar-biaxial setups, the usage of cruciform specimens results in a non-trivial stress and strain distribution of the specimen including its gauge area.

Although even planar-biaxial isothermal LCF tests at room temperature, *e.g.*, References 5 through 7, or elevated temperature, *e.g.*, References 4, 8 through 14, are relatively rare, the superimposed temperature changes of a temperature cycle additionally increase the experimental effort substantially. Up to date, just a few planar-biaxial TMF tests using cruciform specimens were reported so far, for example, on steel^[15,16] and Waspaloy.^[17]

In this work, the planar-biaxial TMF deformation and lifetime behavior of two batches of Inconel 718 were studied for a temperature interval of 400 °C to 630 °C using cruciform specimens. In total, eleven mechanical strain-controlled experiments were performed under proportional loading conditions using biaxial strain ratios $\Phi = -1.0, 0.6, 1.0$. The results were compared with uniaxial TMF reference tests on the same materials. The influence of the multiaxiality on the deformation behavior and the lifetime was evaluated using a modified approach based on the crack opening displacement strain range approach of Itoh and Sakane *et al.*^[18] and the Crossland^[19] equivalent stress amplitude. Additionally, the crack initiation mechanism was investigated and the crack paths of the main cracks were presented.

A. Lifetime Descriptions

For uniaxial mechanical strain-controlled TMF loads, the lifetime N_f depends on the mechanical strain amplitude $\varepsilon_{a,\text{mech}}$, which is the sum of the elastic $\varepsilon_{a,\text{el}}$ and plastic $\varepsilon_{a,\text{pl}}$ strain amplitude (Eq. [3]). Also, the correlation between the elastic $\varepsilon_{a,\text{el}}$ and plastic $\varepsilon_{a,\text{pl}}$ strain amplitude with the lifetime is frequently expressed by exponential functions like the Basquin^[20] (Eq. [4]) and Manson-Coffin^[21–23] (Eq. [5]) approaches using the

materials Young's modulus E and material lifetime parameters σ_f' , b , ε_f' , and c .

$$\varepsilon_{a,\text{mech}} = \varepsilon_{a,\text{el}} + \varepsilon_{a,\text{pl}} \quad [3]$$

$$\varepsilon_{a,\text{el}} = \frac{\sigma_f'}{E} (2N_f)^b \quad [4]$$

$$\varepsilon_{a,\text{pl}} = \varepsilon_f' (2N_f)^c \quad [5]$$

This lifetime description has previously been applied to IN718 under TMF load. In a work of Sun and Yuan,^[2] which included uniaxial TMF In-Phase (IP) and Out-of-Phase (OP) tests of IN718, the Manson-Coffin Basquin curves were found to be intersecting at 0.6 pct mechanical strain amplitude or a lifetime of around 1200 cycles^[2] while cycling the temperature between 300 °C and 650 °C with a cycle duration of 180 seconds. At higher strain amplitudes than 0.6 pct, the lifetime of the IP tests was lower than for OP loading and vice versa for lower strain amplitudes. Deng *et al.*^[24] performed uniaxial IP and OP TMF tests in a temperature interval between 350 °C and 650 °C, which resulted in lifetimes in the range of 70 and 3,000 cycles. Here, the IP tests gained lower lifetimes for the same mechanical strain amplitude compared to the OP tests. The same effect was found by Nitta and Kuwabara^[25] with a point of intersection of around 10^4 cycles.

When the material is not only loaded uniaxially, but multiaxially with more than one principal loading direction, the influence of the change of the loading condition on the lifetime has to be considered. For such loading cases, many models use a strain and stress tensor and calculate a load parameter, for example, a stress, strain, or energy dimension. In some cases, this load parameter is also scaled by an extra parameter to make its value equivalent to an uniaxial load.

In this investigation, a strain-based lifetime correlation, which is a modified version of the crack opening displacement (COD) strain range approach of Sakane *et al.*,^[4,14,18,26] was applied to the experimental results. This approach consists of an equivalent strain amplitude $\varepsilon_{\text{COD},a}$ (Eqs. [6] and [7]) by using the maximum principal strain amplitude $\varepsilon_{I,a}$ and the strain amplitude of the second surface direction $\varepsilon_{II,a}$ or the biaxial ratio Φ . The influence of the multiaxiality is considered by the parameter m' . One scaling parameter β is used to transfer the loading parameter to an uniaxial equivalent.

$$\varepsilon_{\text{COD},a} = \beta(2 - \Phi)^{m'} \varepsilon_{I,a}^* \quad [6]$$

$$\varepsilon_{I,a}^* = \begin{cases} \varepsilon_{I,a} & \text{for } -1 \leq \Phi \leq 0 \\ (\Phi + 1)\varepsilon_{I,a} & \text{for } 0 < \Phi \leq 1 \end{cases} \quad [7]$$

The model was previously applied to perform a strain-based lifetime correlation of planar-biaxial LCF results of IN718, presented by the authors in Reference 12.

On the side of stress-based approaches, the Crossland model^[19] (Eq. [8]) was used to calculate an equivalent stress of a multiaxial stress state. Here, the octahedral shear stress amplitude $\Delta\tau_{\text{oct}}/2$ and the maximum hydrostatic stress component $\sigma_{\text{h,max}}$ within a cycle were used, as well as a model parameter α .

$$\sigma_{\alpha,\text{Crossland}} = \frac{\Delta\tau_{\text{oct}}}{2} + \alpha\sigma_{\text{h,max}} \quad [8]$$

This approach already showed a good lifetime correlation for planar-biaxial LCF tests at temperatures of 400 °C and 630 °C for IN718 in another work of the authors.^[27] To perform the calculations, the multiaxial stress distribution has to be known for the specimen. Hence, finite element (FE) analysis is needed including a proper deformation model.

II. EXPERIMENTAL DETAILS

A. Material

The studied batches of nickel-base superalloy IN718 were supplied in forged, solution annealed, and two-step aged conditions. The heat treatment processes were slightly optimized for their particular applications. While this investigation focused on one material batch of a gas turbine disk (material A), one test was performed using the material of an aviation disk (material B).

Quasi-static, uniaxial LCF, and planar-biaxial LCF material properties of the batches at the minimum and maximum temperatures of the TMF temperature cycle of 400 °C and 630 °C were presented by the authors in a recent study.^[12] The results of warm-tensile tests showed that the quasi-static strength of material B was slightly higher compared to material A. The average grain size of the batches with 8 μm , or 11 according to ASTM E112, was comparable for both batches. Electron Backscatter Diffraction (EBSD) and X-ray diffraction (XRD) measurements revealed that there was no texture. Thus, for this investigation, an isotropic material behavior was adopted.

B. Planar-Biaxial TMF Tests

In this investigation, eleven proportional mechanical strain-controlled planar-biaxial TMF tests were performed (Table I). Ten tests were conducted using material A, and one was performed on material B.

The temperature cycle had minimum and maximum temperatures of 400 °C and 630 °C. The constant cycle duration of 250 s resulted in a constant temperature rate of 1.84 K/s.

The two independent principal mechanical strains of the surface plane in the gauge section ε_1 and ε_2 were available for load control. The mechanical strain ratio for each axis was $R_\varepsilon = -1$. Regarding the mechanical cycles, the same duration of 250 seconds and constant strain rates were applied for each test. All tests were performed with proportional multiaxial loading, specifically with

Table I. Planar-Biaxial TMF Test Parameters^[28,29]

No	Mat	Normalized Principal Mechanical Strain Amplitudes		Biaxial Strain Ratio Φ	Temperature Phase Shift to Mechanical Axes I and II
		$\varepsilon_{I,a}$ [pct]	$\varepsilon_{II,a}$ [pct]		
1	A	0.535	0.535	1	IP
2	A	0.535	0.535	1	OP
3	A	0.467	0.467	1	IP
4	A	0.883	0.883	-1	IP, OP
5	A	0.500	0.500	1	OP
6	A	0.500	0.500	1	IP
7	A	1.000	1.000	-1	IP, OP
8	A	0.400	0.400	1	IP
9	B	0.683	0.410	0.6	OP
10	A	0.400	0.400	1	OP
11	A	0.603	0.362	0.6	OP

biaxial ratios Φ of -1 (shear), 0.6, or 1 (equi-biaxial). Different mechanical strain amplitudes $\varepsilon_{I,a}$ and $\varepsilon_{II,a}$ were investigated, each resulting in slightly different strain rates in combination with the fixed cycle duration. The temperature cycles were either IP or OP relative to the mechanical axes. In the case of the shear tests, the first axis was IP and the second OP. For the tests with biaxial ratios $\Phi > 0$, both axes were either IP or OP.

The lifetime was defined by a drop of a force amplitude of one of both axes of at least 10 pct relative to a stabilized force amplitude. If no stabilization occurred, a 10 pct drop relative to the beginning of the turning point before failure was considered.

The planar-biaxial tests were carried out on a servo-hydraulic test rig Instron 8800 (Figure 1(a)) using cruciform-shaped specimens. The test rig contained two orthogonal axes I and II with four independently controllable actuators with a maximum axial force capacity of 250 kN.

The cruciform specimens had four arms with clamp sections, a ring, and a gauge area in the center. From the end of one arm to the opposite one, the length was 196 mm. The gauge area had a thickness of 1.6 mm and a diameter of 15 mm. Various biaxial strain states were applied in the gauge area by radial forces acting on the specimen's arms. The planar-biaxial strain state was measured using a planar-biaxial extensometer with high-temperature ceramic rods (Figure 1(b)) with a gauge length of 12.5 mm. The temperature was measured by a thermocouple type K spot-welded in the specimens' center on the side of the extensometer. The heat was induced on the other side of the specimen using an induction coil, which was powered by a high-frequency generator. To gain higher cooling rates, the clamps were continuously water-cooled.

Since the mechanical strain of both axes had to be accessed for the performance of TMF tests and only the total strain can be measured, the total strain had to be compensated by the thermal strain induced by the temperature changes. Therefore, the thermal strain was fitted during multiple temperature cycles as a function of

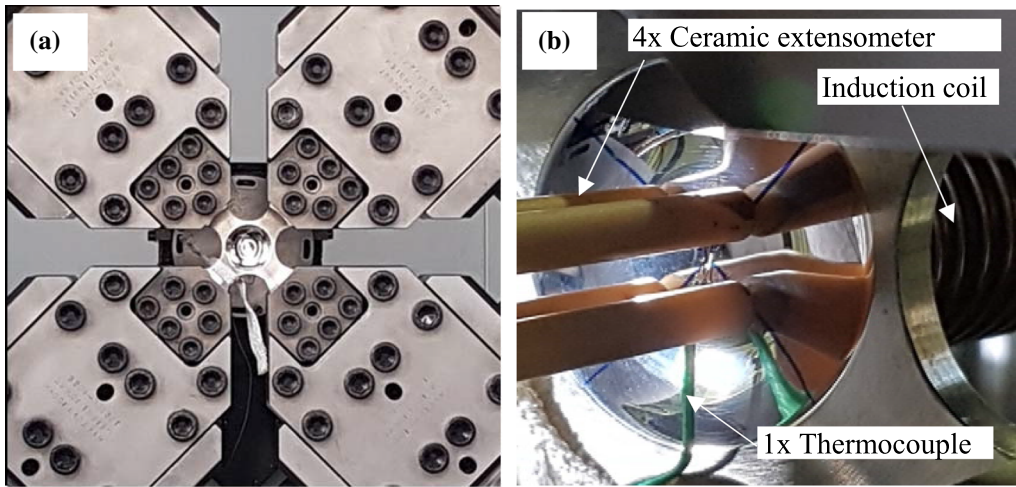


Fig. 1—(a) Planar-biaxial test rig (a) in the clamping section with a mounted cruciform specimen and removed induction coil and (b) with focus on the gauge area from the other side with the applied induction coil. The blue lines with two applied ceramic arms mark the axes (Color figure online).

temperature by a polynomial for each axis, while the specimen was in a forceless condition. Later in the planar-biaxial TMF tests with mechanical load, the thermal strains were continuously subtracted from both total strains to obtain the mechanical strains of both axes.

For an evaluation of the temperature distribution within a temperature cycle and additional numerical analyses, the dynamic heat field of a black-painted specimen was measured using a thermal camera.

The planar-biaxial high-temperature setup and the cruciform fatigue specimens were already the subject of previous investigations on IN718, but also of other superalloys and steels. A first equi-biaxial thermo-mechanical in-phase fatigue test was already performed successfully on the superalloy Waspaloy using the same setup by Kulawinski *et al.*^[17]

C. Uniaxial Reference TMF Tests

Uniaxial mechanical strain-controlled TMF tests were performed IP and OP with various mechanical strain amplitudes with a constant strain ratio $R_\epsilon = -1$. To gain a wider database of TMF tests, the same temperature cycle with peak values of 400 °C and 630 °C was chosen, as well as the cycle duration of 250 seconds was kept constant. All tests were conducted using IN718 of batch A.

In this uniaxial setup, only one mechanical strain was measured and controlled. The transverse strain of the surface was calculated by an effective Poisson ratio ν and a rule-of-mixture (Eq. [9]) proposed by Bannatine *et al.*,^[30] while the plastic Poisson ratio ν_{pl} was set to 0.5 and the elastic Poisson ratio ν_{el} was provided by the material supplying companies. The resulting biaxial ratios of the uniaxial TMF tests were slightly different from each other and in a range of $\Phi = -\nu \approx -0.3 \dots -0.5$.

$$\nu = \frac{\nu_{el}\epsilon_{el} + \nu_{pl}\epsilon_{pl}}{\epsilon_{el} + \epsilon_{pl}} \quad [9]$$

The tests were performed using a servo-hydraulic universal testing system MTS Landmark 100 accordingly to ASTM-E2368. The uniaxial specimens had a gauge length of 16 mm and a gauge diameter of 7 mm. Heating was performed inductively, and the strain was measured using a high-temperature extensometer with a gauge length of 12 mm.

III. RESULTS AND DISCUSSION

A. Temperature Distribution of the Cruciform Specimens

The dynamic temperature fields of a temperature cycle are shown in Figure 2 at the times of the maximum and minimum temperature. Due to the water-cooled clamps, the specimens conducted the heat from the specimens' centers through the arms into the clamp sections.

The thermal gradient induced slightly compressive mean stresses in the center by a thermal expansion gradient.

Focusing on the gauge area, the temperature distributions at the highest tested temperature of 630 °C along three different paths, which are drawn in Figure 2(a), are presented in Figure 3. The indicated temperature drop in the center was induced by the welded thermocouple, *i.e.*, by its geometry in combination with the lower heat emission coefficient, and is therefore not relevant. Because the emission coefficient of the black-painted specimen was adjusted to match the temperature measured by the thermocouple, the real temperature values could slightly differ from the measured one. Nevertheless, the homogeneity of the temperature field within the gauge area with a gradient of 12 K at 630 °C was found to be suitable for the conduction of TMF tests. Additionally, the temperatures were low enough that they did not yield relevant local temperature-induced phase transformation of γ'' - to δ -phase for the subjected test times.

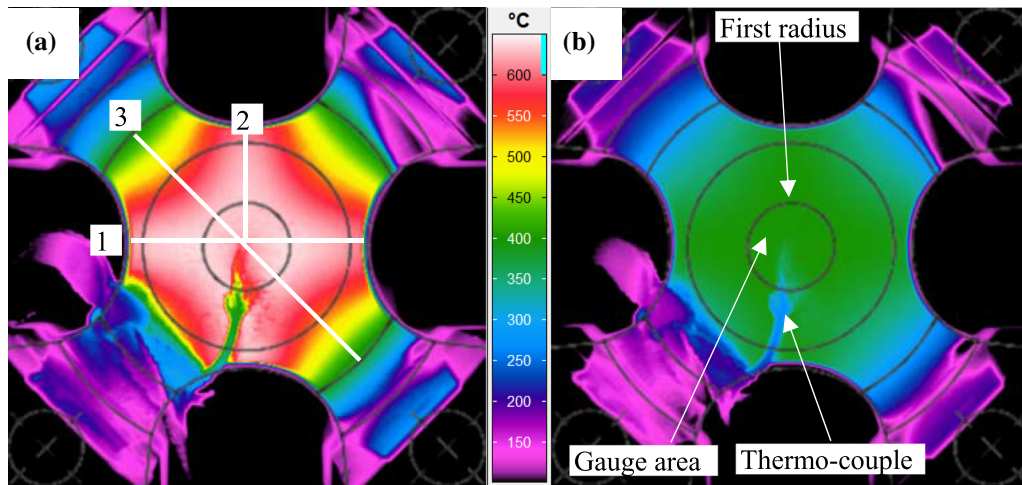


Fig. 2—Temperature distribution of a cruciform specimen within a TMF cycle at its peak temperatures of (a) 630 °C (including measurement lines for Fig. 3) and (b) 400 °C. The specimens' geometrical contours are overlaid. In the gauge area, the temperature was higher than in the specimens' arms. In the center, the spot-welded thermocouple is visible.

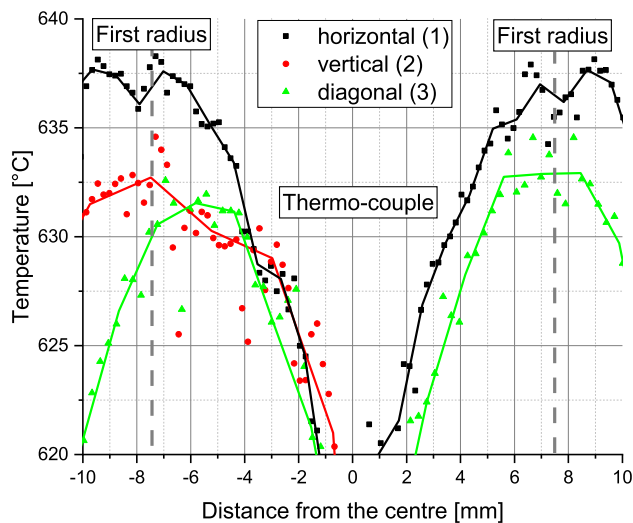


Fig. 3—Temperature gradient along three different paths (presented in Fig. 2) in the gauge area.

The temperature homogeneity of the gauge area was analyzed in depth with multiple thermocouples welded on the front and back side and a thermal camera by Kulawinski *et al.* for isothermal^[9] and thermo-mechanical^[17] planar-biaxial fatigue testing using the same setup and a cruciform specimen of Waspaloy. In these investigations, the difference between two thermocouples on the front and back side was lower than 3 K and, thus, the setup was found to be suitable for TMF testing.

B. Cyclic Deformation Behavior

1. Uniaxial tests

The curves of the normalized stress amplitudes over the number of cycles for the uniaxial TMF-IP and OP tests are shown in Figure 4. For both loading cases, the

material showed pronounced cyclic softening. While the softening effect got weaker with increasing number of cycles, a stabilization of the stress amplitudes occurred only for lower mechanical strain amplitudes $\epsilon_a \leq 0.91$ pct (normalized) for IP loading.

The softening behavior of IN718 was comparable to the results of the investigations of Deng *et al.*^[24] for uniaxial TMF tests between 350 °C and 650 °C as well as to the tests in a temperature interval of 300 °C and 650 °C of Sun and Yuan.^[31]

In Figure 5, the IP and OP TMF tests of a certain mechanical strain amplitude are compared with LCF tests of the maximum and minimum temperature of the same mechanical strain amplitude. Here, the stress amplitudes of the TMF-IP and -OP tests were between the isothermal tests. At high mechanical strain amplitude (Figure 5(b)), the stress amplitudes were closer to amplitudes of the LCF tests of the maximum temperature. Besides that, the stress amplitudes of the IP and OP tests were comparable with each other for the majority of the cycles.

The normalized mean stresses *vs.* the number of cycles are presented in Figure 6. In contrast to LCF tests,^[12] the material developed significant mean stresses over the number of cycles. For the mechanical strain-controlled tests, the mean stresses were negative for IP and positive for OP loads. In addition, the absolute values were increasing over the number of cycles. It is worth mentioning, that the tests of the highest mechanical strain amplitudes had lower absolute mean stress values in the first cycles in comparison to their lower counterparts.

The same trend of the mean stress development was also presented in investigations by Deng *et al.*,^[12] Sun and Yuan,^[31] and Schlesinger *et al.*^[32]

2. Planar-biaxial fatigue tests

The normalized force amplitudes of the planar-biaxial TMF tests are presented in Figure 7. Although only the reaction forces applied on the specimens' arms were

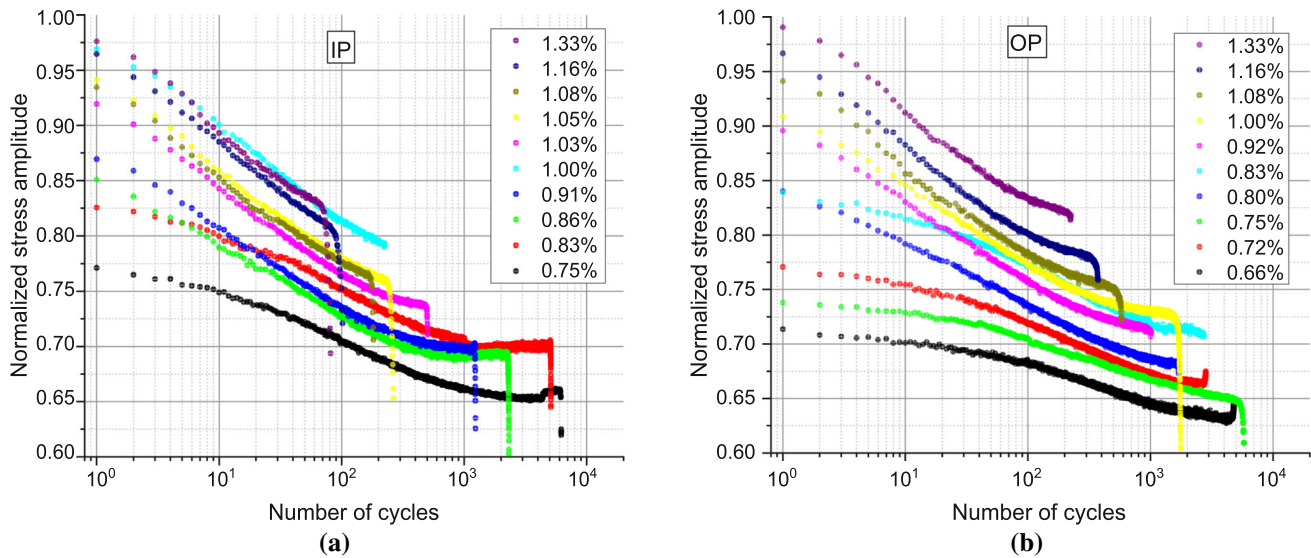


Fig. 4—Normalized stress amplitudes vs. the number of cycles of the uniaxial TMF tests under (a) in-phase and (b) out-of-phase loading. The labels indicate the normalized mechanical strain amplitudes. Reprinted and modified with permission from Refs. [28, 29].

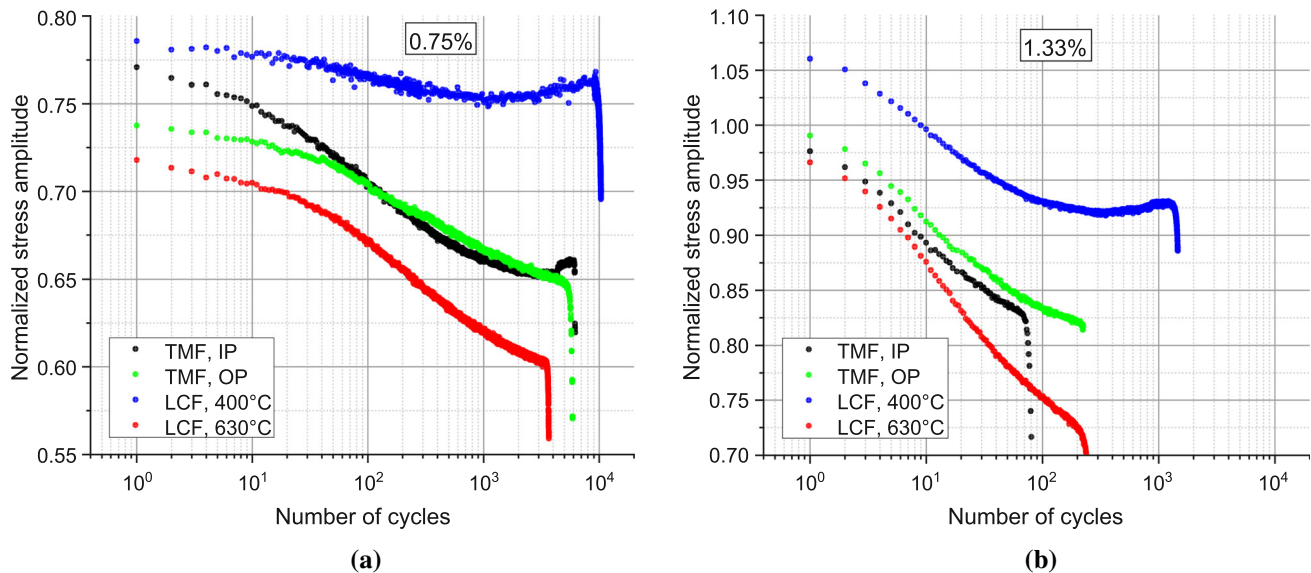


Fig. 5—Comparison of IP- and OP-TMF and isothermal LCF tests at temperatures of 400 °C and 630 °C with normalized mechanical strain amplitudes of (a) 0.75 pct (low) and (b) 1.33 pct (high). The LCF tests had a constant strain rate of 10^{-3} /s. Data were taken with permission from Refs. [28, 29].

measurable and the stresses are not that easily accessible without the utilization of numerical simulations, the decrease of the force amplitudes over the number of cycles showed the cyclic softening behavior under planar-biaxial TMF loading. For equi-biaxial loads, the force amplitudes of both axes were overall similar, what was expected due to the symmetrical loading conditions.

In the shear case, the stress amplitudes of both axes were different from each other (Figure 7(c)). The axis which applied positive strain in the tensile direction in the first cycle had a higher force amplitude throughout the whole test, whereas the strain amplitude of the second axis was lower. In comparison to the equi-biaxial

load, the shear load caused significantly lower force amplitudes, even for the higher mechanical strain amplitudes in each axis.

Such an influence of multiaxiality was also reported for planar-biaxial LCF tests at 400 °C and 630 °C performed by the authors.^[12] This deformation behavior can be explained by common equivalent stress hypotheses, like that of von Mises. Here, under shear loading, the stresses are lower since no hydrostatic stresses exist.

The normalized mean forces of the planar-biaxial TMF tests are presented in Figure 8. In the tests with biaxial ratios ϕ of 1.0 and 0.6, both axes of a test were either IP (Figure 8(a)) or OP (Figure 8(b)) relative to the temperature cycle. Here, the same mean stress

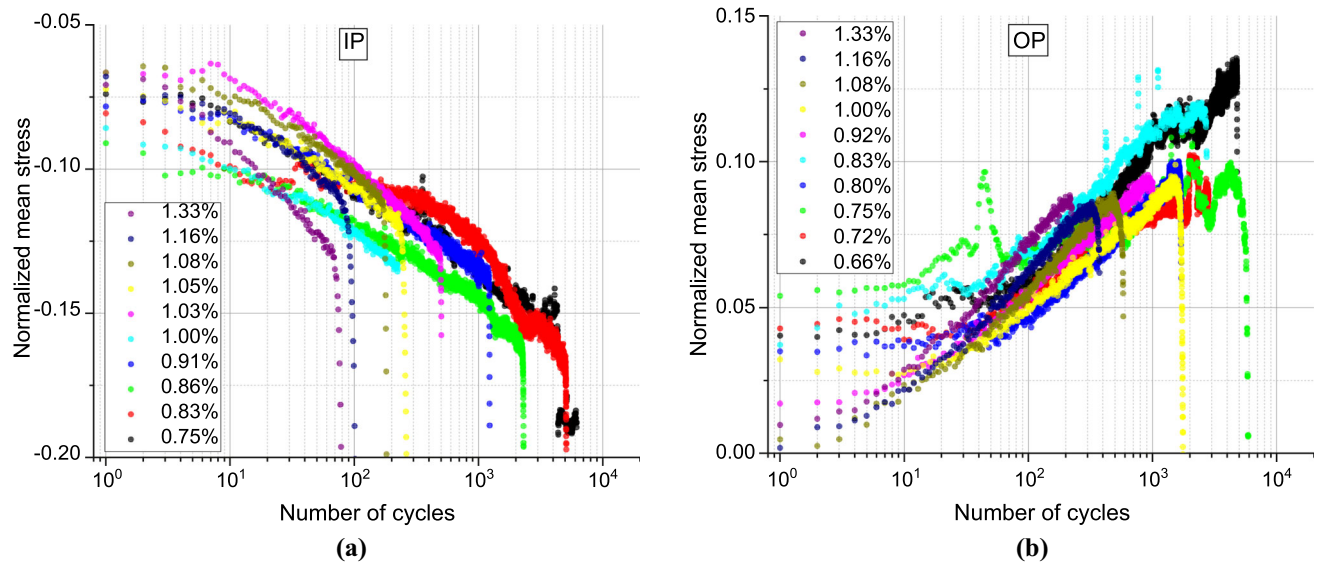


Fig. 6—Normalized mean stress vs. the number of cycles of the uniaxial (a) IP- and (b) OP-TMF tests. Data were taken with permission from Refs. [28, 29].

development as in the uniaxial TMF tests can be noticed with negative mean forces for the IP load and positive mean forces for the OP load. In addition, for the tests with a biaxial ratio ϕ of 0.6, both axes developed a similar trend.

Regarding the shear tests with a biaxial ratio ϕ of -1.0 (Figure 8(c)), one axis was IP and the other OP with the temperature cycle. While the OP axis showed a positive mean force development, the IP axis started with a negative mean force, which was also slightly increasing over the number of cycles. The shear test with a normalized mechanical strain amplitude of 0.883 pct was interrupted and restarted, which resulted in the negative offset of the mean forces, but had only a small influence on the force amplitudes (Figure 7(c)).

C. Fatigue Lifetimes

1. Uniaxial loading

The lifetimes of the uniaxial TMF tests are presented in Figure 9(a) together with data of isothermal LCF tests at 400 °C and 630 °C on the same material, presented in another investigation by the authors.^[12] At high mechanical strain amplitudes, the IP tests had lower lifetimes than the respective OP tests. Here, the lifetimes of the OP tests were around the lifetime of the 630 °C LCF tests. For low amplitudes, the OP tests had lower lifetimes than the equivalent IP tests. The point of intersection was found to be close to a lifetime of around 1000 cycles. The lifetimes of the 400 °C LCF tests were higher than the TMF tests in all studied cases. Nevertheless, the higher lifetimes of the TMF-IP tests tended to be between the lifetimes of the isothermal fatigue tests of both temperatures.

The results are similar to the results of the investigations of Sun and Yuan,^[2] Deng *et al.*,^[24] and Nitta and Kuwabara.^[25] In all investigations with a mechanical strain ratio of $R_\epsilon = -1$, the IP tests gained lower

lifetimes for high mechanical strain amplitudes compared to the OP tests. The same behavior was also found for other polycrystalline superalloys, such as Nimonic 90^[33] or MAR-M247 LC.^[34]

In superalloys under TMF loading, the number of cycles to failure is mainly driven by crack propagation.^[35,36] A possible explanation for the different behaviors of the two TMF cases is that in the low lifetime regime, crack propagation under IP loading is higher than under OP loading. This was demonstrated for a temperature cycle between 427 °C and 649 °C with IP and OP loading and a strain range of 1.15 pct by Kim and Van Stone,^[37] and additionally for superalloy RR1000 by Pretty *et al.*^[38] In the high lifetime regime, this effect may not be the dominant factor, whereas the developed mean stresses (Figure 6), higher oxidation damage, and a lack of crack closure could be more relevant for lifetime reduction of the OP tests.^[39]

In the Manson-Coffin plot with the plastic strain amplitude calculated at half lifetime (Figure 9(b)), a non-linearity in the double-logarithmic relation was found like it is well-known for uniaxial LCF tests at temperatures of 427 °C or lower.^[40,41] Hence, the TMF lifetimes were fitted using a dual-slope Coffin-Manson approach and slightly different Basquin parameters. At higher lifetimes or lower mechanical strain amplitudes, a change of the Manson-Coffin exponent c to more negative values occurred. Like for LCF tests, this effect can be explained by a transition of the materials' deformation behavior.^[40,41] The deformation is supposed to be homogeneously distributed in the microstructure for higher strain amplitudes, while for lower ones, the plastic deformation occurred only in selected grains.^[41]

The Manson-Coffin exponents c of the OP tests were more negative than the IP counterparts for the same lifetimes. The trend of the different exponents can furthermore be found in the investigations of Sun and

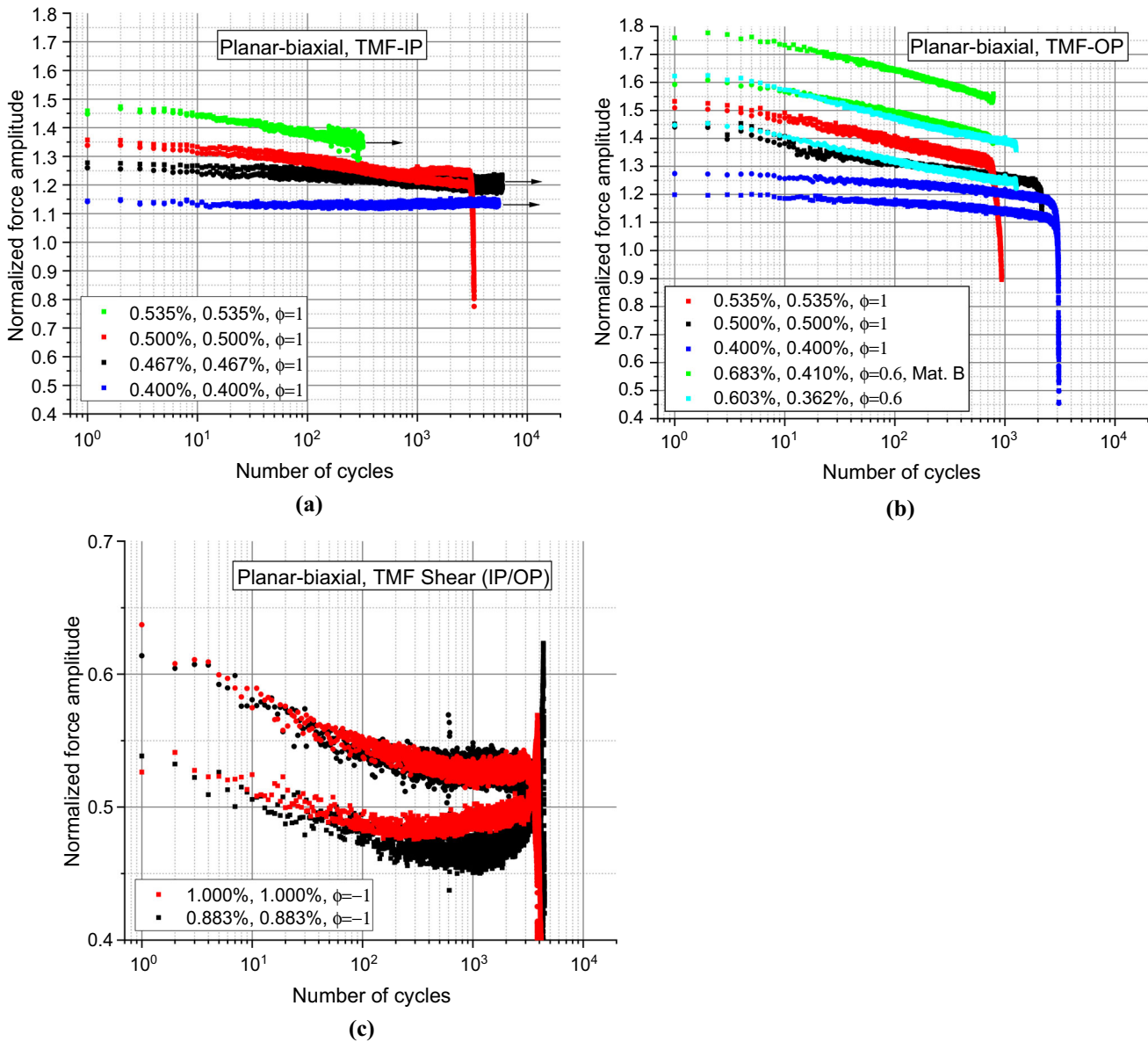


Fig. 7—Normalized force amplitudes of the planar-biaxial TMF tests with (a) IP loading, (b) OP loading, and (c) shear with IP and OP loading. For each test, the force amplitudes of both axes are drawn in a similar color. Three of four equi-biaxial IP tests were aborted by extensometer displacement, marked with arrows. Reprinted and modified with permission from Refs. [28, 29] (Color figure online).

Yuan.^[2] Interestingly, the lifetimes of the OP tests at higher strain amplitudes and the IP tests at lower strain amplitudes could be fitted with one Coffin-Manson fit, what can be explained by a common fatigue mechanism responsible for the lifetime determination. Besides that, one OP test at high lifetime was in line with this description.

The Basquin parameters were fitted for each interval and differed slightly from each other, mainly due to scattering.

Besides of the ability to fit the lifetime for each test condition using the Manson-Coffin and Basquin approach, the mechanical strain amplitudes were not sufficient to describe the influence of the different temperatures under LCF loading and the impact of the TMF loading conditions, as also observed for other

superalloys, such as René 80.^[42] To integrate the influence of various temperatures on the lifetime calculation, other approaches have to be considered, also to take non-symmetrical nature of environmental TMF damage into account, as reported by Lancaster *et al.*^[43]

Besides that, also a Basquin life equation was used for the prediction of longer TMF tests for RR1000^[44,45] in combination with a crack growth model, while different phase shifts between axial strain and temperature were tested.

While a complete model including the temperature influence has still to be developed or adapted, the uniaxial description could be suitable to evaluate the influence of the multiaxial loading on the TMF lifetime, while the main TMF parameters are hold constant. Focusing on the multiaxial material behavior, the

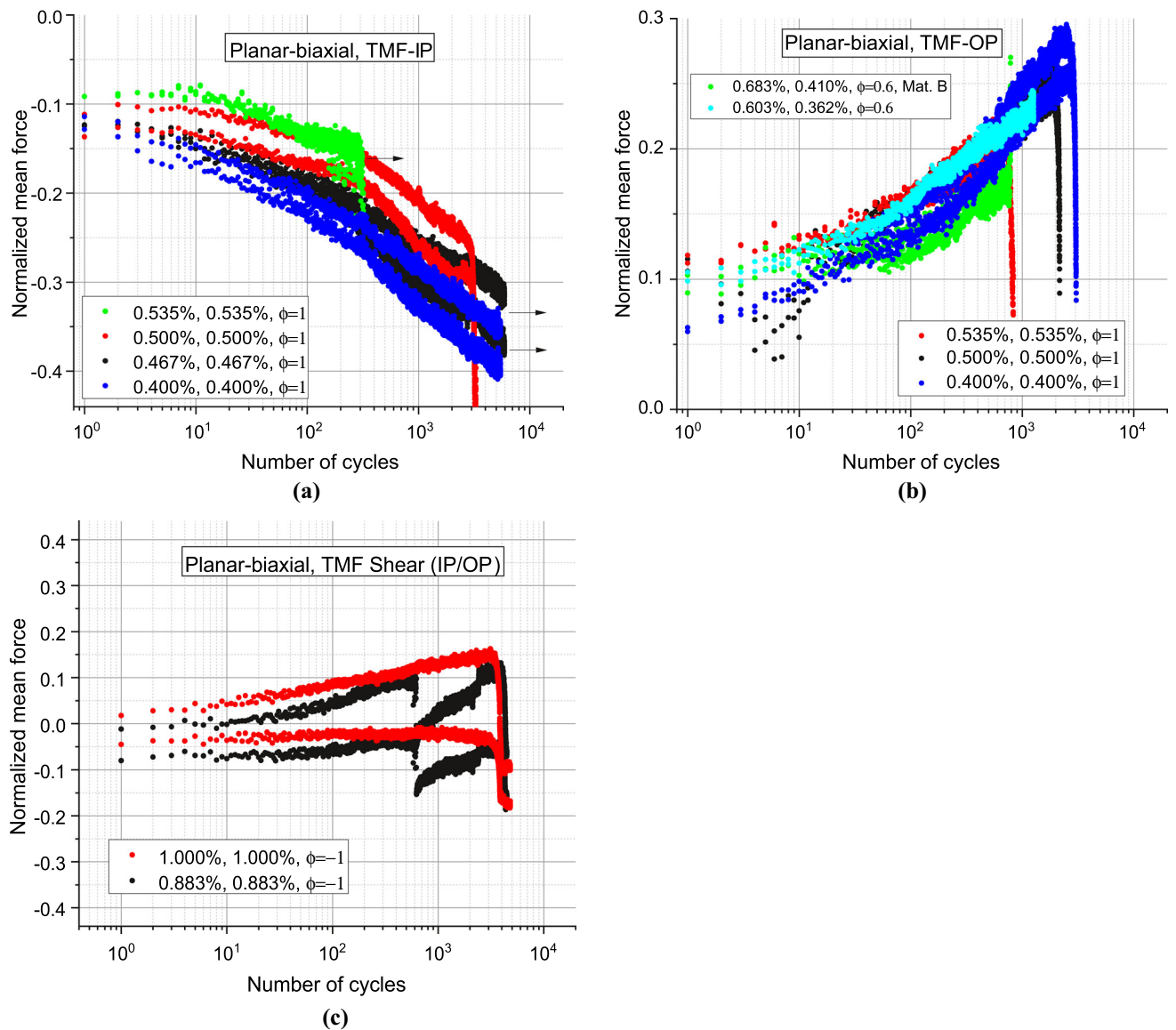


Fig. 8—Normalized mean forces of the planar-biaxial (a) IP, (b) OP, and (c) shear TMF tests. For each test, the force amplitudes of both axes are drawn in the same color. Reprinted and modified with permission from Refs. [28, 29] (Color figure online).

influence of the strain or temperature rate on the lifetime was not investigated due to the constant cycle duration of 250 seconds. The influence of shorter cycle durations on the lifetime will be presented in a further study.

2. Multiaxial loading

Out of the eleven proportional planar-biaxial TMF tests, eight tests were performed until the end of the lifetime with the initiation of a visible technical crack. Among the four equi-biaxial IP tests, three tests were interrupted by an unintended displacement of extensometer arms on the specimens' surface throughout the tests with no visible technical cracks initiated.

Regarding a strain-based lifetime description, the modified COD strain amplitudes vs. lifetimes are shown in Figure 10(a). For the description, two different parameter sets were used, one for the low and the other for the high lifetime regime. The transition between the two sets

was at 1600 cycles. The equivalent strain amplitude was then used in combination with the uniaxial IP and OP Manson-Coffin and Basquin fit, to predict the lifetime (Figure 10(b)). The shear tests were predicted using the uniaxial OP Manson-Coffin and Basquin fit.

The model correlated the planar-biaxial and uniaxial tests of $\Phi \geq -v$ nearby the corresponding uniaxial IP and OP tests and yielded a conservative lifetime prediction, besides of one equi-biaxial OP test, which had a prediction deviation of 3. The interrupted equi-biaxial IP tests were not over-predicted. Regarding the shear tests, the lifetimes were conservative compared to both the uniaxial IP and OP tests. Even if no uniaxial TMF reference data of material B were available, the lifetime description was comparable with the results of material A.

Using FE simulation, a coupled deformation model was considered to describe the cyclic material effects subjected to different uniaxial and multiaxial loading

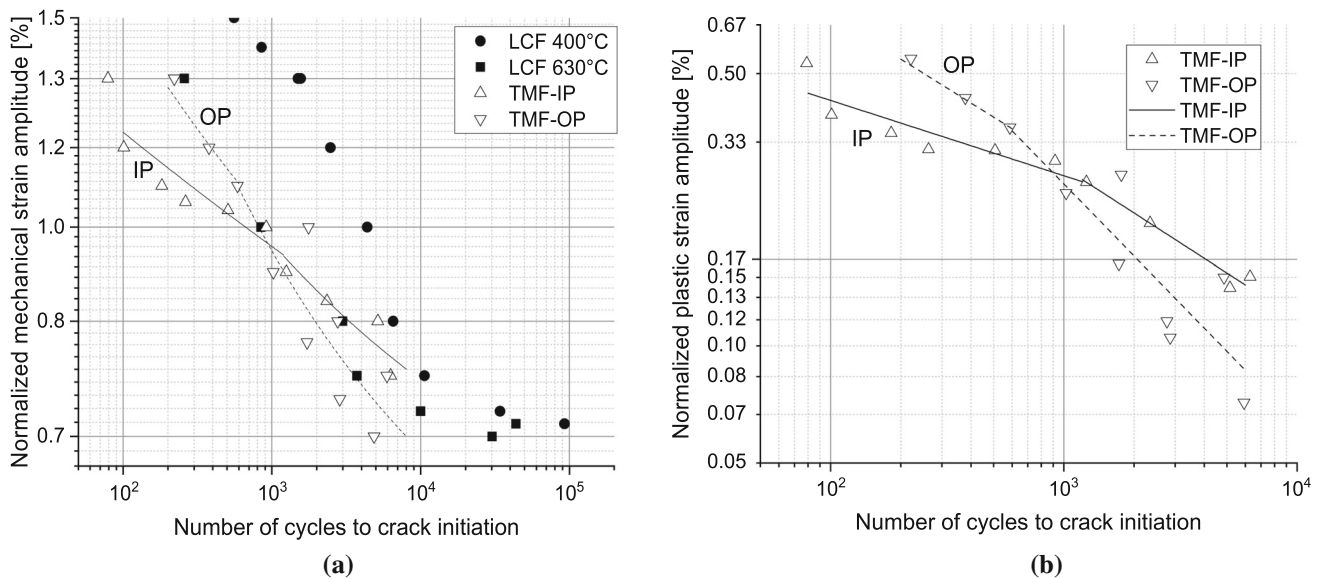


Fig. 9—Uniaxial TMF lifetime with fits for IP and OP loading (a) in comparison to LCF tests of 400 °C and 630 °C of the authors^[12] and (b) Coffin-Manson plot with the normalized plastic strain amplitude vs. lifetime. Data were taken with permission from Refs. [28, 29].

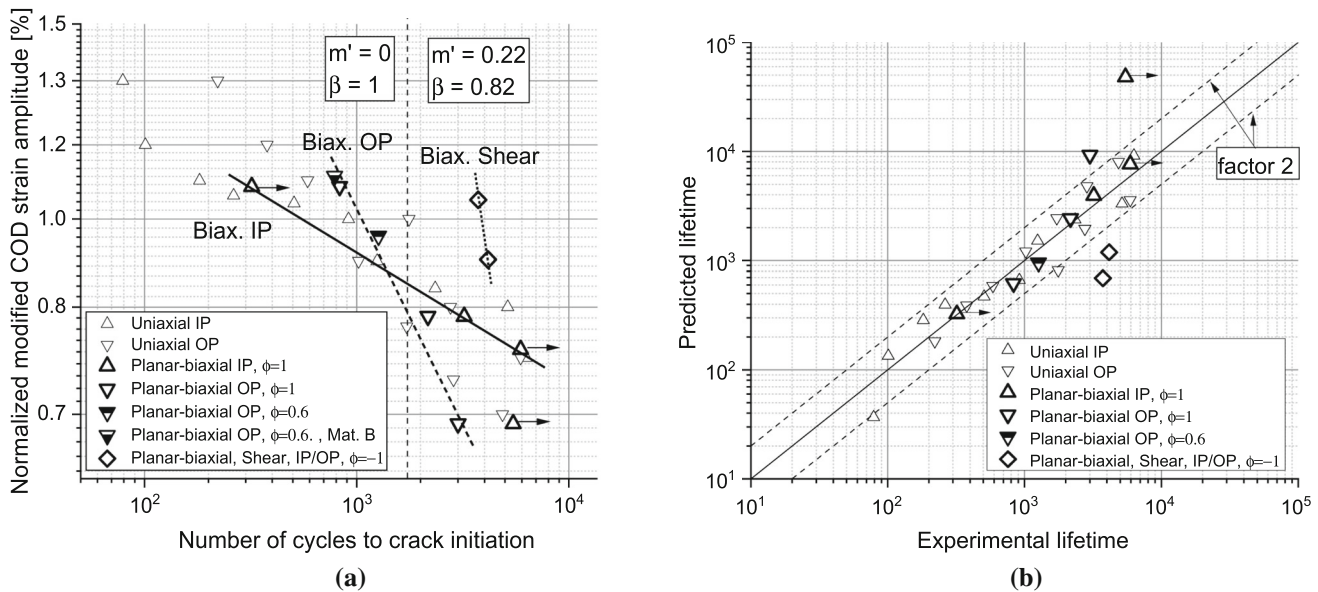


Fig. 10—(a) Normalized modified COD equivalent strain amplitude vs. lifetime of all TMF tests using two different parameter sets. Regressions of the equi-biaxial IP and OP tests are close to the uniaxial lifetimes. (b) Predicted vs. experimental lifetime for all TMF tests of material A. Data were taken with permission from Refs. [28, 29].

conditions. In detail, the model consisted of the approaches of Chaboche for the kinematic hardening, Perzyna for the rate dependency, and Voce for the isotropic hardening. The material parameters of the deformation model were calibrated on uniaxial isothermal CLCF tests and were already used for the deformation calculation of planar-biaxial LCF tests.^[27] With this model, the deformation behavior of the tests was simulated until stabilized force amplitudes were calculated.

Considering the planar-biaxial TMF tests, the stress and strain distributions were calculated for one equi-biaxial IP and OP until stabilization with the same parameter set.

With the calculated stress distribution of the gauge area, the lifetime of the uniaxial, one equi-biaxial TMF, and LCF tests at 630 °C were correlated using the Crossland equivalent stress amplitude with a precision of factor 3 (Figure 11). One equi-biaxial TMF-IP test, which was a run-out, could have been non-conservatively predicted.

As an alternative stress-based equivalent, the model of Sines *et al.*^[46] was tested without satisfactory correlation. Also, the energy-based model of Smith–Watson–Topper^[47] was not successfully applied regarding a multiaxial TMF lifetime prediction.

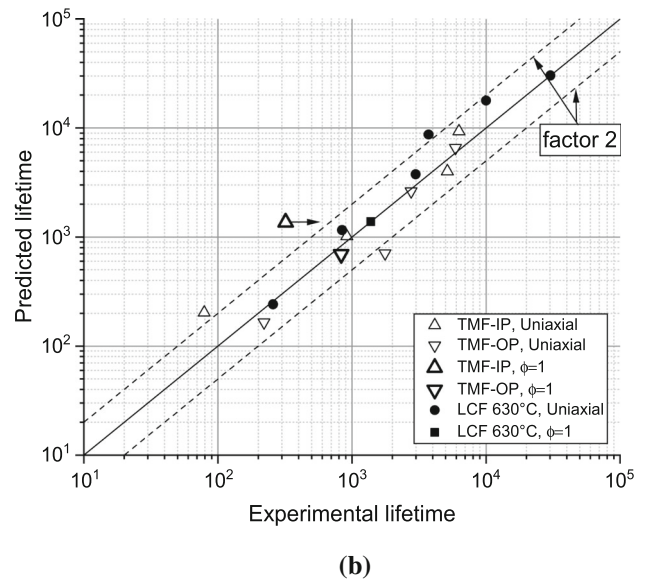
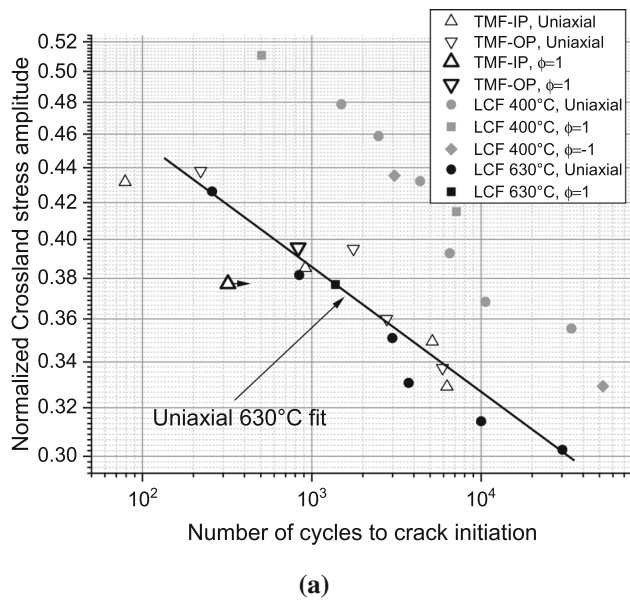


Fig. 11—(a) Normalized Crossland equivalent stress amplitude vs. lifetime for material A for the tests with performed simulations and (b) predicted vs. experimental lifetime. Uniaxial and planar-biaxial LCF tests were taken from another publication of the authors,^[12] and data were taken with permission from Refs. [28, 29].

Multiaxial non-proportional TMF loading conditions were not investigated in this work. For such loading conditions, the presented approaches with amplitudes of scalar values are most likely not suitable. The influence of more complex non-proportional planar-biaxial TMF loading conditions on the deformation and lifetime behavior of IN718 may be the subject of further investigations.

D. Crack Initiation and Crack Paths

The paths of the cruciform specimens' main cracks and their initiation positions are presented in Figure 12. Fatigue crack initiation occurred within the gauge area or at the beginning of the first radius at the surface. For three out of four equi-biaxial IP tests with the numbers 1, 3, and 8, no crack was visible.

For many tests, more than one fatigue crack initiation position was observed in the main crack surface, as presented for two cruciform specimens in Figure 13. Interestingly, the most initiation locations on the main cracks were found for the OP tests with a biaxial ratio ϕ of 0.6 when the main cracks grew along the first radius. Regarding the other tests, less fatigue crack initiation sites were detected. In some tested specimens with technical cracks, no exact crack initiation position was found, like for specimen no. 10.

Due to the different oxidation colors of the crack surfaces, some information may be gathered regarding the temperature and time exposure. While some initiated cracks or positions were most likely to be exposed for longer times at high temperatures, like the right crack with a darker color in Figure 13(a), other positions or cracks were not that long exposed and had a brighter color. Here, the initiation sites at the beginning of the radius of the OP tests with a biaxial ratio ϕ of 0.6 had

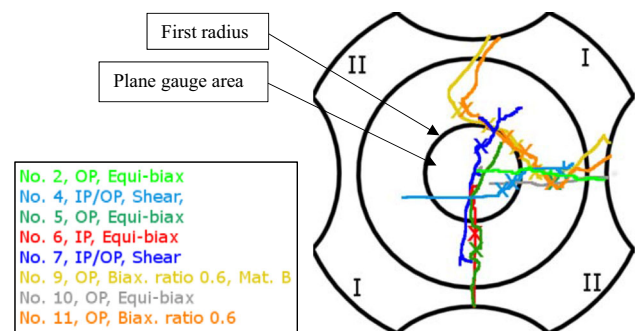


Fig. 12—Crack paths of the main cracks of the cruciform TMF specimens. The mechanical axes are labeled I and II. Positions of fatigue crack initiation are marked by "x." Reprinted and modified with permission from Ref. [29].

the darkest color and therefore probably the cracks which were initiated first.

Crack initiation, also of secondary cracks (Figure 14), took place at non-metallic inclusions in the surface area as previously reported for room and high-temperature fatigue tests.^[48–51] In the presence of elevated temperatures, the oxidation of carbides resulted in a volume expansion and caused substantial deformation of the surrounding matrix.^[48] In the case of the occurrence of multiple fatigue crack initiation spots on the main crack, a combination of the separate cracks had to occur. These positions were visible as step-like structures (Figures 13(a) and (b)).

The initiation of multiple secondary cracks at carbides supports the assumption, that the crack growth phase is the most relevant phase for the TMF lifetime determination, compared to the initiation process, as reported by References 35, 36.

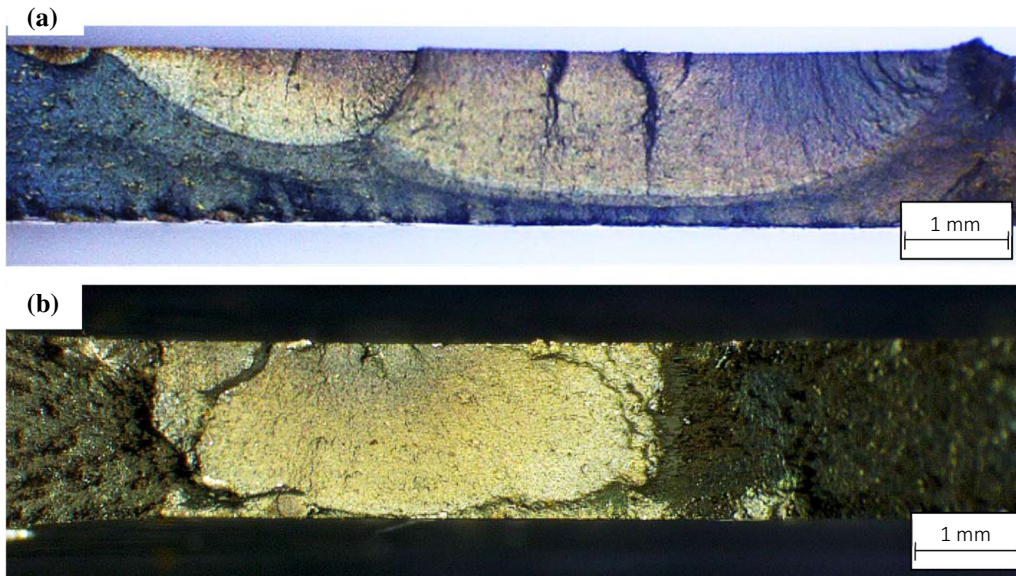


Fig. 13—Multiple initiation spots on the surface of the main crack of the specimen (a) No. 9 (biaxial ratio 0.6, OP, material B) (reprinted with permission from Ref. [29]) and (b) No. 4 (shear, TMF, material A).

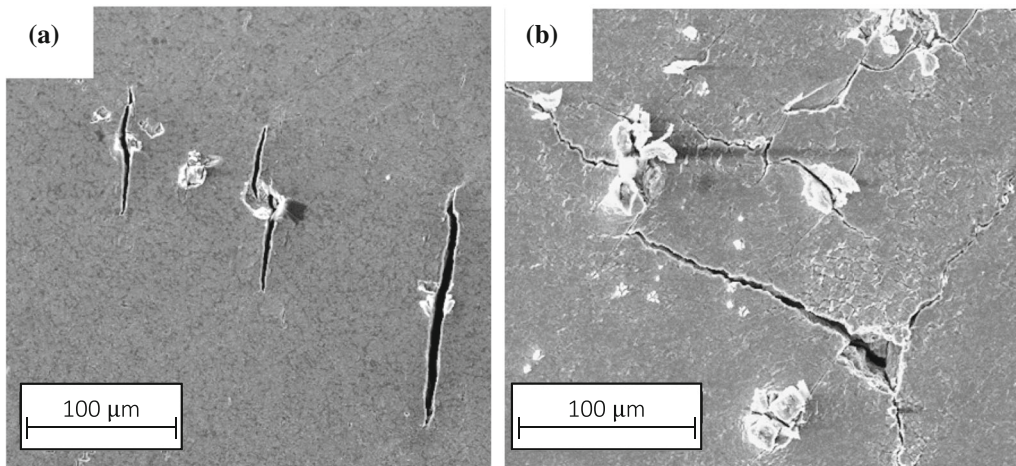


Fig. 14—Surface of the gauge area of the specimens (a) No. 5 (equi-biaxial, OP, material A) and (b) No. 7 (shear, IP/OP, material A) after the end of the lifetime. Secondary cracks are visible, which were initiated at carbides. The pictures were aligned in analogy to Fig. 12.

IV. CONCLUSIONS

The proportional planar-biaxial TMF behavior of Inconel 718 was investigated for various biaxial ratios Φ for a temperature cycle with minimum and maximum temperatures of 400 °C and 630 °C, respectively. The main conclusions of this investigation are as follows:

- IN718 showed cyclic softening under proportional TMF loading.
- Axes under IP loading developed negative and axes under OP loading had positive mean stresses.
- An equivalent strain amplitude based on a modified model of Itoh *et al.*^[14,18,26] yielded a satisfying lifetime prediction for the tests with a biaxial ratio $\Phi \geq -\nu$ in combination with the uniaxial Manson-Coffin and Basquin IP and OP fits. The shear tests were predicted too conservative.

- The Crossland equivalent stress amplitude was a successful parameter for a stress-based TMF lifetime correlation. Here, the TMF lifetimes of two simulated planar-biaxial and uniaxial TMF tests were correlated by the uniaxial LCF fit at 630 °C, which was the cycles' maximum temperature.
- Initiation of fatigue cracks occurred at the gauge areas' surfaces at non-metallic inclusions.

ACKNOWLEDGMENTS

The results were generated in the German-funded project “Lifing Methods, Multiaxial and Anisothermal (LEBEMAN)” within the German research association

FVV (Forschungsvereinigung Verbrennungskraftmaschinen e. V.) under the project number 1288 and supported by the German Federal Ministry for Economic Affairs and Energy (BMWi) through the AiF (German Federation of Industrial Research Associations e. V.), with the project number IGF 26EW, based on a decision taken by the German Bundestag. The authors like to thank the accompanying work group with industrial project partners for their constructive discussions and continuous support. We would especially like to thank the project's chairperson Dr. Hartmut Schlums (Rolls-Royce Deutschland Ltd & Co KG) for his contribution.

CONFLICT OF INTEREST

On behalf of all authors, the corresponding author states that there is no conflict of interest.

FUNDING

Open Access funding enabled and organized by Projekt DEAL.

OPEN ACCESS

This article is licensed under a Creative Commons Attribution 4.0 International License, which permits use, sharing, adaptation, distribution and reproduction in any medium or format, as long as you give appropriate credit to the original author(s) and the source, provide a link to the Creative Commons licence, and indicate if changes were made. The images or other third party material in this article are included in the article's Creative Commons licence, unless indicated otherwise in a credit line to the material. If material is not included in the article's Creative Commons licence and your intended use is not permitted by statutory regulation or exceeds the permitted use, you will need to obtain permission directly from the copyright holder. To view a copy of this licence, visit <http://creativecommons.org/licenses/by/4.0/>.

REFERENCES

1. N.E. Waldren, M.J. Percy, and P.B. Mellor: *Proc. Inst. Mech. Eng.*, 1965, vol. 180, pp. 111–30.
2. J. Sun and H. Yuan: *Int. J. Fatigue*, 2019, vol. 120, pp. 228–40.
3. J. Sun, H. Yuan, and M. Vormwald: *Int. J. Fatigue*, 2020, vol. 135, 105486.
4. S. Zhang and M. Sakane: *Int. J. Fatigue*, 2007, vol. 29, pp. 2191–99.
5. S. Ackermann, D. Kulawinski, S. Henkel, and H. Biermann: *Int. J. Fatigue*, 2014, vol. 67, pp. 123–33.
6. S. Henkel, J. Fischer, L. Balogh, T. Ungar, and H. Biermann: *J. Phys.: Conf. Series*, IOP Publishing, p. 12042.
7. S. Ackermann, T. Lippmann, D. Kulawinski, S. Henkel, and H. Biermann: *Frattura ed Integrità Strutturale*, 2015, vol. 9.
8. D. Kulawinski, M. Hoffmann, T. Lippmann, G. Lamprecht, A. Weidner, S. Henkel, and H. Biermann: *J. Mater. Res.*, 2017, vol. 32, pp. 4411–23.
9. D. Kulawinski, S. Henkel, D. Holländer, M. Thiele, U. Gampe, and H. Biermann: *Int. J. Fatigue*, 2014, vol. 67, pp. 212–19.
10. D. Kulawinski, S. Henkel, H. Biermann, D. Holländer, M. Thiele, and U. Gampe: *International Conference on Multiaxial Fatigue & Fracture (ICMFF10)*, 2013.
11. D. Kulawinski, M. Hoffmann, A. Weidner, T. Lippmann, G. Lamprecht, S. Henkel, and H. Biermann: *Fatigue Fract. Eng. Mater. Struct.*, 2017, vol. 40, pp. 909–23.
12. M. Böcker, H. R. Babu, S. Henkel, M. Raddatz, U. Gampe, and H. Biermann: *Fatigue Fract. Eng. Mater. Struct.*, 2022.
13. A. Erbe, F. Conrad, K.M. Kraemer, C. Kontermann, M. Bianchini, D. Kulawinski, and M. Oechsner: *Proc. Struct. Integr.*, 2022, vol. 38, pp. 192–201.
14. T. Itoh, M. Sakane, and M. Ohnami: *J. Eng. Mater. Technol.*, 1994, vol. 116, pp. 90–98.
15. L. Cui, P. Wang, H. Hoche, A. Scholz, and C. Berger: *Mater. Sci. Eng. A*, 2013, vol. 560, pp. 767–80.
16. A. Samir, A. Simon, A. Scholz, and C. Berger: *Int. J. Fatigue*, 2006, pp. 643–51.
17. D. Kulawinski, A. Weidner, S. Henkel, and H. Biermann: *Int. J. Fatigue*, 2015, vol. 81, pp. 21–36.
18. T. Itoh, M. Sakane, T. Hata, and N. Hamada: *Int. J. Fatigue*, 2006, vol. 28, pp. 459–66.
19. D.J. White, B. Crossland, and J.L. Morrison: *Trans. Natl. Res. Inst. Met.*, 1978, pp. 167–71.
20. O.H. Basquin, ed.: *The exponential law of endurance tests*, 1910.
21. L.F. Coffin: *Appl. Mater. Res.*, 1962, 129ff.
22. L.F. Coffin and J.F. Tavernelli: *Trans. Metall. Soc. AIME*, 1959, pp. 794–806.
23. L.F. Coffin: *Trans. Am. Soc. Mech. Eng. N. Y.*, 1954, vol. 76, pp. 931–50.
24. W. Deng, J. Xu, Y. Hu, Z. Huang, and L. Jiang: *Mater. Sci. Eng. A*, 2019, vol. 742, pp. 813–19.
25. A. Nitta and K. Kuwabara: *Elsevier Applied Science Publishers, High Temperature Creep-Fatigue*, 1988, pp. 203–22.
26. N. Hamada, M. Sakane, and M. Ohnami: *J. Soc. Mater. Sci. Jpn.*, 1985, vol. 34, pp. 214–20.
27. H. Ramesh Babu, M. Böcker, M. Raddatz, S. Henkel, H. Biermann, and U. Gampe: *Proceedings of the ASME Turbo Expo 2021, Turbomachinery Technical Conference and Exposition*, 2021.
28. *Proceedings of the FVV Autumn Conference 2021, FVV Information Sessions Turbomachinery*, 2021, pp. 445–78.
29. *Lebensdauermethoden, multiaxial und anisotherm (LEBEMAN): FVV Final Report No. 1288*, 2021.
30. J. Bannatine, J. Comer, and J. Handrock: Research supported by the University of Illinois. *Englewood Cliffs, NJ, Prentice Hall*, 1990, vol. 1990, p. 286.
31. J. Sun and H. Yuan: *Int. J. Fatigue*, 2019, vol. 119, pp. 89–101.
32. M. Schlesinger, T. Seifert, and J. Preussner: *Int. J. Fatigue*, 2017, vol. 99, pp. 242–49.
33. M. Marchionni, H. Klingelhöffer, H. J. Kühn, T. Ranucci, and K. Matzak: *Key engineering materials*, Trans Tech Publ, pp. 347–50.
34. S. Guth, S. Doll, and K.-H. Lang: *Proc. Eng.*, 2014, vol. 74, pp. 269–72.
35. E.E. Affeldt, J. Timm, and A. Bennett: *Fatigue under Thermal and Mechanical Loading: Mechanisms, Mechanics and Modelling*, Springer, Berlin, 1996, pp. 159–68.
36. J. Bressers, J. Timm, S.J. Williams, A. Bennett, and E. Affeldt: *ASTM Spec. Tech. Publ.*, 1996, vol. 1263, pp. 56–67.
37. K.S. Kim and R. H. Vanstone: Elevated temperature crack growth, 1992.
38. C.J. Pretty, M.T. Whitaker, and S.J. Williams: *Materials (Basel, Switzerland)*, 2017, vol. 10, p. 34.
39. H. Sehitoglu: *Thermo-mechanical fatigue life prediction methods*, ASTM International, 1992.
40. T.H. Sanders, R.E. Frishmuth, and G.T. Embley: *Metall. Trans. A*, 1981, vol. 12, pp. 1003–10.
41. A. Cruzado, S. Lucarini, J. Llorca, and J. Segurado: *Int. J. Fatigue*, 2018, vol. 107, pp. 40–48.

42. B. Buchholz, U. Gampe, and T. Beck: *Turbo Expo: Power for Land, Sea, and Air*, American Society of Mechanical Engineers, pp. 187–96.
43. R.J. Lancaster, M.T. Whittaker, and S.J. Williams: *Mater. High Temp.*, 2013, vol. 30, pp. 2–12.
44. J. Jones, M. Whittaker, R. Lancaster, and S. Williams: *MATEC Web of Conferences*, EDP Sciences, p. 19001.
45. V. Gray, J.P. Jones, M.T. Whittaker, R.J. Lancaster, C.J. Pretty, and S.J. Williams: *Int. J. Fatigue*, 2022, vol. 156, 106631.
46. G. Sines and G. Ohgi: *J. Eng. Mater. Technol.*, 1981.
47. K. Smith: *J. Mater.*, 1970, vol. 5, pp. 767–78.
48. T. Connolly, M.J. Starink, and P.A. Reed: *Superalloys*, 2000, vol. 2000, pp. 435–44.
49. J. Belan: *Metallurgija*, 2015, vol. 54, pp. 59–62.
50. P.R. Bhowal, D. Stolz, A. M. Wusatowska-Sarnek, and R. Montero: *Superalloy 2008, The Minerals Metals & Materials Society (TMS)*, 2008.
51. D. Texier, J.-C. Stinville, M.P. Echlin, S. Pierret, P. Villechaise, T.M. Pollock, and J. Cormier: *Acta Mater.*, 2019, vol. 165, pp. 241–58.

Publisher's Note Springer Nature remains neutral with regard to jurisdictional claims in published maps and institutional affiliations.